Journal of
Materials Chemistry C

PAPER

View Article Online
View Journal | View Issue

Check for updates

Cite this: J. Mater. Chem. C, 2018, 6, 11416

New heterobimetallic Au(I)–Pt(II) polyynes achieving a good trade-off between transparency and optical power limiting performance†

Zhuanzhuan Tian,[a] Xiaolong Yang,[a] Boao Liu,[a] Daokun Zhong,[a] Guijiang Zhou *[a] and Wai-Yeung Wong[b]

Received 27th June 2018,
Accepted 1st October 2018

DOI: 10.1039/c8tc03157f

rsc.li/materials-c

Two series of new heterobimetallic Au(I)–Pt(II) polyynes have been easily synthesized by cross-coupling under mild conditions. The absorption profiles of these two series of Au(I)–Pt(II) polyynes are quite similar. However, the Au(I)–Pt(II) polyynes with a 1,4-bis(diphenylphosphino)benzene ligand show stronger triplet (T_1) emission and superior optical power limiting (OPL) performance than the corresponding Au(I)–Pt(II) polyynes with a 1,3-bis(diphenylphosphino)propane ligand. Hence, the 1,4-bis(diphenylphosphino)benzene ligand is more effective than the 1,3-bis(diphenylphosphino)propane ligand for optimizing the transparency and OPL ability of OPL materials. When compared with the corresponding homometallic Pt(II) polyynes, these heterobimetallic Au(I)–Pt(II) polyynes display a blue shift in their absorption spectra, showing better transparency in the visible-light region. Besides, these heterobimetallic Au(I)–Pt(II) polyynes show stronger OPL ability than their corresponding homometallic Pt(II) polyynes as well as the state-of-the-art OPL material C_{60}, demonstrating their enormous application potential in the nonlinear optics field. In brief, the introduction of Au(I) precursors with tetrahedral diphosphine ligands into the backbone of Pt(II) polyynes can simultaneously achieve enhanced transparency and high OPL ability for OPL materials, providing a new strategy to optimize OPL materials.

Introduction

Lasers are widely used in many fields, such as material processing, surgery, military activities, *etc.*[1] However, inevitable damage is caused to human eyes and optical sensors when exposed suddenly to strong laser beams. So, studies of optical power limiting materials have become more urgent.[2,3] Until now, many types of OPL materials have been established, such as fullerenes,[4] metallophthalocyanines,[5,6] metalloporphyrins,[7,8] organic materials,[9–12] graphenes,[13,14] carbon nanotubes[15] and so on. Most of these materials exhibit high OPL performance and fast response speed and allow flexible chemical modifications. However, their strong absorptions beyond 400 nm result in poor transparency in the visible-light region,[16] restricting their practical applications. Obviously, solving the conflict between good transparency and high OPL ability of OPL materials presents a critical issue in the nonlinear optics field. Due to the interaction between metal centers and organic acetylene ligands, organometallic acetylide compounds show unique properties. In addition, Yang's group reported that novel molecular skeletons and self-assembly structures formed by the new Pt(II) acetylenes also show intriguing properties.[17–20] Hence, organometallic acetylides are widely applied in multiple fields.[21–24] Importantly, they have great potential in coping with this conflict considering their good trade-off between transparency and OPL performance for OPL materials.[25,26]

Recently, Pt(II), Au(I), Hg(II) and Pd(II) acetylide compounds as high-performance OPL materials have been developed.[16,27–35] Among them, Pt(II) acetylide compounds have been extensively investigated due to their good transparency in the visible-light region and high OPL ability. With respect to Pt(II) acetylides, Pt(II) polyynes have the advantages of enhanced OPL ability and good film-forming ability for device fabrication,[36,37] suggesting their greater practical application potential in the OPL field. However, the transparency of Pt(II) polyynes is inferior to that of Pt(II) acetylides due to the red shift of the absorption band caused by polymerization.[27,34] To solve this problem, researchers have explored a new strategy in which Hg(II) or Pd(II) ions were

[a] MOE Key Laboratory for Nonequilibrium Synthesis and Modulation of Condensed Matter, State Key Laboratory for Mechanical Behavior of Materials, Department of Chemistry, School of Science, State Key Laboratory for Mechanical Behavior of Materials, Xi'an Jiaotong University, Xi'an 710049, P. R. China. E-mail: zhougj@mail.xjtu.edu.cn; Fax: +86-29-8266-3914

[b] Department of Applied Biology and Chemical Technology, The Hong Kong Polytechnic University, Hung Hom, Hong Kong, P. R. China

† Electronic supplementary information (ESI) available: Synthetic details for organic ligands, Au^I acetylides and some photophysical data. See DOI: 10.1039/c8tc03157f

introduced into the backbone of homometallic Pt(II) polyynes.[34] It is worth noting that introducing Hg(II) ions into the backbone of homometallic Pt(II) polyynes with fluorene-based ligands can not only improve their transparency, but also offer them comparable OPL performance with that of homometallic Pt(II) polyynes. However, introducing Pd(II) ions into the backbone of homometallic polyynes cannot significantly enhance the OPL properties and transparency. The high toxicity of Hg(II) ions[38,39] and the poor effect of introducing Pd(II) ions into the backbone of Pt(II) polyynes limit the application of these ions in OPL materials development. Therefore, effective strategies have to be developed for optimizing the transparency and OPL performance of Pt(II) polyynes.

Au(I) acetylide compounds usually exhibit excellent transparency in the visible-light region,[27,31,40] which can be attributed to the weak interaction between the 5d orbitals of the Au(I) centers and the π orbitals of the organic ligands. Goswami *et al.* reported one thienyl-carbazole-based Au(I) acetylide with high transparency comparable to its organic ligand.[27] This is because the absorption band of this Au(I) acetylide only shows a very slight red-shift compared with that of its organic ligand. In addition, the transparency of the concerned OPL materials can be successfully improved by introducing tetrahedral diphosphine ligands to the backbone of the Pt(II) polyyne due to their conjugation-breaking ability. Recently, we have reported a series of new Au(I) polyynes with tetrahedral diphosphine ligands with excellent transparency in the visible-light region and some of them even outperform C_{60} as OPL materials.[40] So, the introduction of Au(I) ions and tetrahedral diphosphine ligands into homometallic Pt(II) polyynes should be a promising protocol to reduce the red shift effect after polymerization. On the basis of these advantages, by combining monomeric Pt(II) acetylides and the dinuclear Au(I) complex precursors with tetrahedral diphosphine ligands, two series of new heterobimetallic Au(I)–Pt(II) polyynes have been developed. Compared with the corresponding homometallic Pt(II) polyynes, these new polyynes can not only show better transparency, but also achieve stronger optical limiting performances by effectively maintaining the density of the metal atom of the polyyne chain. Hence, the results of the concerned polyynes should provide a new means for achieving comprehensive optimization between good transparency and high OPL ability.

Experimental

General information

Commercially available reagents were used directly as received. The solvents were refined through a normative process under dry nitrogen for use. All reactions were completed under a nitrogen atmosphere. The reactions were monitored by thin-layer chromatography (TLC) using Merck pre-coated aluminum plates. Flash column chromatography and preparative TLC were carried out using silica gel. All Sonogashira reactions were completed using Schlenk techniques under a nitrogen atmosphere.

Physical measurements

All the NMR spectra were measured in $CDCl_3$ solvent using a Bruker AXS 400 MHz NMR spectrometer with the ^1H and ^{13}C NMR chemical shifts quoted relative to $SiMe_4$ and the ^{31}P chemical shifts relative to the 85% H_3PO_4 external standard. Fast atom bombardment (FAB) mass spectra were characterized using a Finnigan MAT SSQ710 system. UV-Vis spectra were recorded on a PerkinElmer Lambda 950 spectrophotometer at 298 K. The photoluminescent (PL) properties were characterized using an Edinburgh Instruments FLS920 fluorescence spectrophotometer. The lifetimes at 298 K for the excited states were measured using a single photon counting spectrometer from Edinburgh Instruments FLS920 with a 360 nm picosecond LED lamp as the excitation source, while those at 77 K were obtained with the excitation from a xenon flash lamp. The low-temperature PL spectra and lifetimes at 77 K were measured by dipping the degassed CH_2Cl_2 solution in a thin quartz tube into a liquid nitrogen Dewar and the data were recorded after allowing it to stand for 3 minutes. The fluorescence quantum yields (Φ_F) were measured in CH_2Cl_2 solutions at 298 K against quinine sulfate in 1.0 M H_2SO_4 as the reference (Φ_F *ca.* 0.56 at 334 nm and *ca.* 0.55 at 365 nm).[41] The molecular weights were determined using Waters 2695 GPC in $CHCl_3$ and estimated by using a calibration curve of polystyrene standards.

Optical power limiting measurements

The optical power limiting properties were characterized by *Z*-scan measurements, which were performed at 532 nm for the Gaussian mode laser beam with a repetition frequency of 20 Hz from a Q-switched Quantel Q-Smart 100 Nd:YAG laser. The laser beam was split into two beams by a beam splitter. One was used as the reference beam, which was directly received by a power detector (D1), and the other was focused with a lens (f = 20 cm) for sample measurement. After starting the position control device, the light beam through the sample was collected immediately by another power detector (D2). The sample to be measured was moved automatically along a rail to change the incident irradiance with its distance (*Z*-position). The incident and transmitted powers were detected simultaneously using D1 and D2, separately. The OPL performance of each solution sample was measured in CH_2Cl_2 with *ca.* 90% transmittance solution filled in a 1 mm quartz cell. OPL devices based on **P1-FLU** and **P2-FLU** were prepared by casting the polystyrene (PS) solution (0.2 g mL^{-1}) in $CHCl_3$ with a *ca.* 1.0 wt% doping level into a PTFE mould, respectively. Then, they were left on a clean bench for 3 days at room temperature to obtain solid plates as prototype OPL devices.

Computational details

Geometrical optimizations were conducted using the popular B3LYP density functional theory (DFT). The basis set used for C, H, O, N and P atoms was 6-311G(d, p), whereas effective core potentials with a LanL2DZ basis set were employed for Au and Pt atoms.[42,43] The energies of the excited states of the complexes were computed by TD-DFT based on all the

ground-state geometries. All calculations were carried out by using the Gaussian 09 program.[44]

Synthesis

Monomeric Pt(II) acetylides (**FLU-Pt-FLU**, **TPA-Pt-TPA** and **CAZ-Pt-CAZ**) were obtained using a modified method.[34,40] **L-P1-Au** and **L-P2-Au** were synthesized as in a published reaction.[45,46] All the synthetic procedures are provided in the ESI.†

A general synthetic procedure for Au(I)–Pt(II) polyynes

Under a N_2 atmosphere, **L-P1-Au**/**L-P2-Au** (1.0 equiv.) and the corresponding Pt(II) acetylides (1.0 equiv.) were mixed in CH_2Cl_2/MeOH (v : v = 2 : 1). Then, sodium methoxide solution (3.0 equiv., 0.3 M) was added. The reaction mixture was kept stirring for 5 h at room temperature. After removing the solvent, the obtained residue was dissolved in a small amount of CH_2Cl_2 and filtered using a syringe filter (PTFE, 0.45 μm) to remove the insoluble part. Then, it was precipitated in MeOH and this procedure was repeated two times. The heterobimetallic Au(I)–Pt(II) polyynes were obtained as an off-white solid.

P1-FLU. (Yield: 56%). ^{1}H NMR (400 MHz, $CDCl_3$): δ (ppm) 7.64–7.58 (m, 8H, Ar), 7.55–7.44 (m, 22H, Ar), 7.21 (m, 6H, Ar), 2.20 (br, 12H, PBu_3), 1.86 (br, 8H, –CH_2–), 1.66 (br, 12H, PBu_3), 1.50–1.44 (br, 12H, PBu_3), 1.25–0.99 (m, 72H, –CH_2–), 0.94 (t, 18H, PBu_3), 0.88–0.84 (m, 12H, –CH_3), 0.57 (br, 8H, –CH_2–); ^{31}P NMR (161.9 MHz, $CDCl_3$): δ (ppm) 42.45, 2.83; GPC: M_n = 2.4 × 10^4 g mol^{-1}, PDI = 1.6 (against polystyrene standards); anal. found: C 60.96, H 5.68.

P1-TPA. (Yield: 60%). ^{1}H NMR (400 MHz, $CDCl_3$): δ (ppm) 7.63–7.46 (m, 22H, Ar), 7.35–7.31 (m, 10H, Ar), 7.10–6.91 (m, 6H, Ar), 6.86–6.79 (m, 10H, Ar), 3.92 (t, 4H, –OCH_2–), 2.12 (br, 12H, PBu_3), 1.76–1.75 (br, 4H, –CH_2–), 1.57–1.54 (m, 12H, PBu_3), 1.46–1.40 (m, 12H, PBu_3), 1.35–1.26 (m, 36H, –CH_2–), 0.93–0.86 (m, 24H, PBu_3 and –CH_3); ^{31}P NMR (161.9 MHz, $CDCl_3$): δ (ppm) 42.44, 2.70; GPC: M_n = 2.7 × 10^4 g mol^{-1}, PDI = 1.3 (against polystyrene standards); anal. found: C 60.96, H 5.68.

P1-CAZ. (Yield: 52%). ^{1}H NMR (400 MHz, $CDCl_3$): δ (ppm) 8.24–8.22 (m, 2H, Ar), 7.96–7.87 (m, 2H, Ar), 7.64–7.48 (m, 26H, Ar), 7.38 (m, 2H, Ar), 7.25–7.19 (m, 4H, Ar), 4.20 (t, 4H, –NCH_2–), 2.23 (br, 12H, PBu_3), 1.83–1.81 (m, 4H, –CH_2–), 1.68 (br, 12H, PBu_3), 1.55–1.47 (m, 12H, PBu_3), 1.33–1.24 (m, 36H, –CH_2–), 0.99–0.94 (t, 18H, PBu_3), 0.89–0.86 (m, 6H, –CH_3); ^{31}P NMR (161.9 MHz, $CDCl_3$): δ (ppm) 42.56, 3.03; GPC: M_n = 2.9 × 10^4 g mol^{-1}, PDI = 1.4 (against polystyrene standards); anal. found: C 60.96, H 5.68.

P2-FLU. (Yield: 55%). ^{1}H NMR (400 MHz, $CDCl_3$): δ (ppm) 7.76–7.72 (m, 6H, Ar), 7.57–7.38 (m, 22H, Ar), 7.22–7.20 (d, 4H, Ar), 2.85 (br, 4H), 2.19 (br, 12H, PBu_3), 1.97–1.88 (br, 10H), 1.66 (br, 12H, PBu_3), 1.52–1.44 (m, 12H, PBu_3), 1.25–1.21 (m, 72H, –CH_2–), 0.94 (t, 18H, PBu_3), 0.87–0.84 (m, 12H, –CH_3), 0.58 (br, 8H, –CH_2–); ^{31}P NMR (161.9 MHz, $CDCl_3$): δ (ppm) 35.18, 2.77; GPC: M_n = 2.1 × 10^4 g mol^{-1}, PDI = 1.3 (against polystyrene standards); anal. found: C 60.96, H 5.68.

P2-TPA. (Yield: 65%). ^{1}H NMR (400 MHz, $CDCl_3$): δ (ppm) 7.71–7.68 (m, 6H, Ar), 7.44–7.42 (m, 8H, Ar), 7.37–7.29 (m, 6H, Ar), 7.16–7.00 (m, 10H, Ar), 6.96–6.78 (m, 14H, Ar), 3.92 (br, 4H, –OCH_2–), 2.81 (br, 4H), 2.12–2.11 (br, 12H, PBu_3), 1.95–1.90 (m, 2H), 1.77 (m, 4H, –CH_2–), 1.57–1.54 (m, 12H, PBu_3), 1.46–1.40 (m, 12H, PBu_3), 1.33–1.26 (m, 36H, –CH_2–), 0.92–0.86 (m, 24H, PBu_3 and –CH_3); ^{31}P NMR (161.9 MHz, $CDCl_3$): δ (ppm) 35.28, 2.65; GPC: M_n = 2.4 × 10^4 g mol^{-1}, PDI = 1.5 (against polystyrene standards); anal. found: C 60.96, H 5.68.

P2-CAZ. (Yield: 58%). ^{1}H NMR (400 MHz, $CDCl_3$): δ (ppm) 8.27–8.17 (m, 2H, Ar), 8.00–7.96 (m, 2H, Ar), 7.75 (m, 8H, Ar), 7.63–7.57 (m, 2H, Ar), 7.46–7.34 (m, 14H, Ar), 7.27–7.20 (m, 4H, Ar), 4.21 (br, 4H, –NCH_2–), 2.85 (br, 4H), 2.23 (br, 12H, PBu_3), 2.00 (br, 2H), 1.84 (br, 4H, –CH_2–), 1.68 (br, 12H, PBu_3), 1.51–1.44 (m, 12H, PBu_3), 1.33–1.24 (m, 36H, –CH_2–), 0.96–0.86 (m, 24H, PBu_3 and –CH_3); ^{31}P NMR (161.9 MHz, $CDCl_3$): δ (ppm) 35.36, 2.94; GPC: M_n = 3.1 × 10^4 g mol^{-1}, PDI = 1.5 (against polystyrene standards); anal. found: C 60.96, H 5.68.

Results and discussion

Synthesis and structural characterization

The synthetic routes to monomeric Pt(II) acetylides (**FLU-Pt-FLU**, **TPA-Pt-TPA** and **CAZ-Pt-CAZ**), **L-P1-Au** and **L-P2-Au** are provided in Scheme S1 (ESI†). Ethynyl aromatic ligands (**L-FLU**, **L-TPA** and **L-CAZ**) are prepared first. Then monomeric Pt(II) acetylides can be easily synthesized through the Sonogashira cross-coupling in high yields. In the ^{1}H NMR spectra of these Pt(II) acetylides, the signals at *ca.* 3.1 ppm are from the alkynyl group of ethynyl aromatic ligands and three sets of multiple peaks in the range of *ca.* 2.2–1.4 ppm are from PBu_3 groups. In their ^{31}P NMR spectra, the peaks at *ca.* 2.8 ppm are attributed to PBu_3 groups. The above results can demonstrate that monomeric Pt(II) acetylides are successfully obtained.

Scheme 1 shows the synthetic pathways of the heterobimetallic Au(I)–Pt(II) polyynes. Using a similar synthetic strategy for homometallic polyynes,[34] these polyynes have been prepared by the cross-coupling between **L-P1-Au**/**L-P2-Au** and the corresponding monomeric Pt(II) acetylides. The chemical structures of these Au(I)–Pt(II) polyynes have been fully characterized by ^{1}H and ^{31}P NMR spectra. In the ^{1}H NMR spectra of these Au(I)–Pt(II) polyynes, the peaks at *ca.* 3.1 ppm from the proton of alkyne groups disappear, compared with those from the monomeric Pt(II) acetylides. Two sets of resonance peaks at *ca.* 2.8 ppm from PBu_3 groups and at *ca.* 42.4 ppm from **L-P1-Au**/**L-P2-Au** can clearly show the simultaneous existence of the *trans*-[$Pt(PBu_3)_2$] unit and **L-P1-Au**/**L-P2-Au** in their ^{31}P NMR spectra. Hence, the above results reveal their successful coupling between **L-P1-Au**/**L-P2-Au** and the corresponding monomeric Pt(II) acetylides. In the ^{1}H NMR spectra of these Au(I)–Pt(II) polyynes, the multiple peaks in the range of *ca.* 1.5–0.8 ppm can be assigned to the *n*-dodecyl groups and the PBu_3 groups in these polyynes. In the ^{1}H NMR spectra of **P1-TPA** and **P2-TPA**, the signals at *ca.* 3.9 ppm can be induced by the protons from the –OCH_2– unit. The signals at *ca.* 4.2 can be ascribed to the –NCH_2– group in the ^{1}H NMR spectra of **P1-CAZ** and **P2-CAZ**. The broad peaks at *ca.* 2.8 ppm come from the –$CH_2CH_2CH_2$– unit of

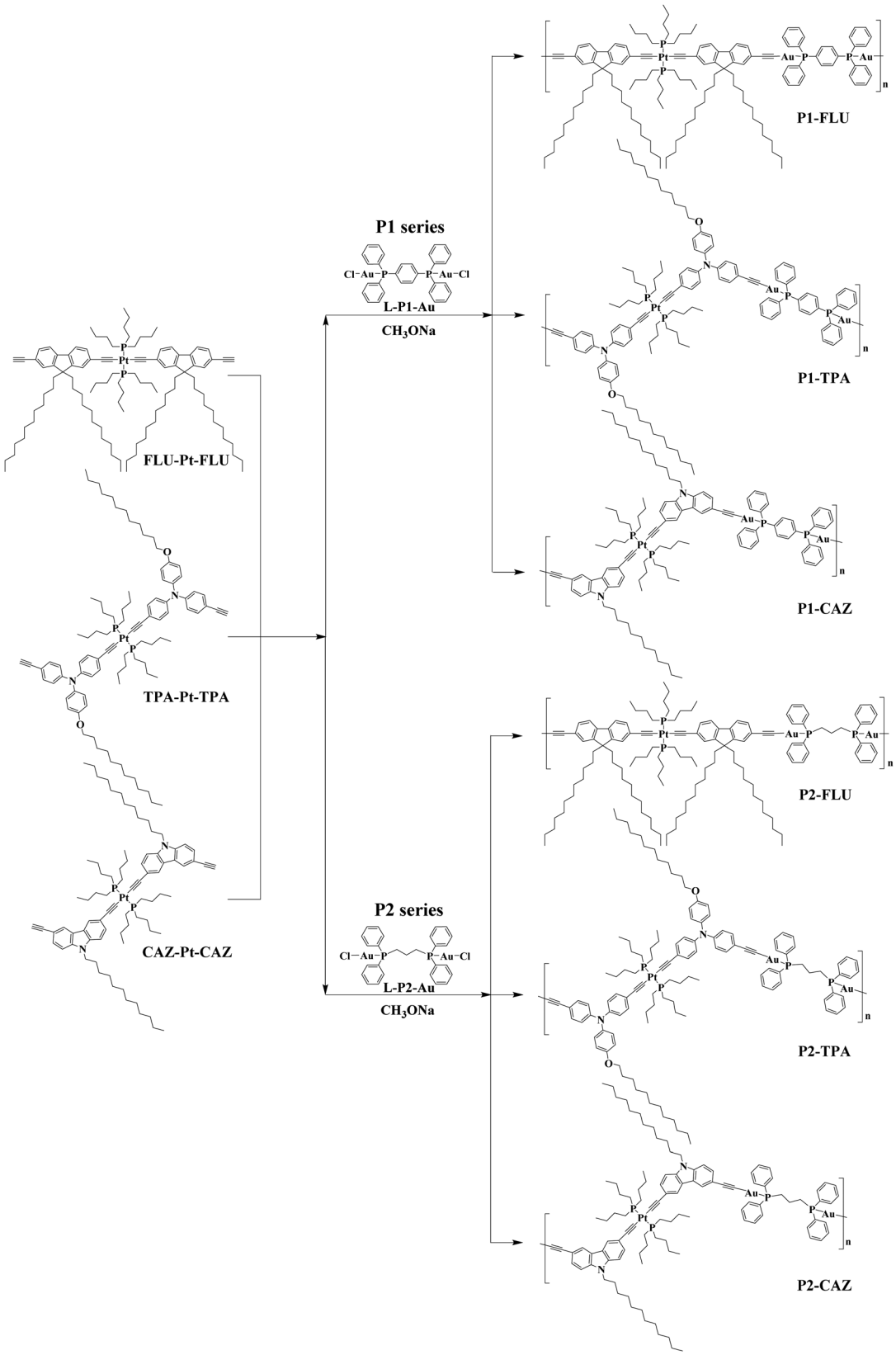

Scheme 1 Synthesis of heterobimetallic Au(I)–Pt(II) polyynes.

L-P2-Au in the ^{1}H NMR spectra of **P2-FLU**, **P2-TPA** and **P2-CAZ**. All these NMR data clearly indicate the successful synthesis of these new heterobimetallic Au(I)–Pt(II) polyynes.

Photophysical properties

The absorption spectra of the Au(I)–Pt(II) polyynes have been characterized in CH_2Cl_2 at 298 K and the corresponding data are summarized in Table 1. Obviously, the maximum absorption wavelengths (λ_{max}) of two series of Au(I)–Pt(II) polyynes (P1 and P2 series, Fig. 1) show a blue shift compared with those of the corresponding homometallic Pt(II) polyynes (Fig. S1 and Table S1, ESI†). Besides, the cut-off absorption wavelengths ($\lambda_{cut\text{-}off}$) of P1 and P2 series show a slight blue shift compared with those of the corresponding homometallic Pt(II) polyynes. When compared with that of the corresponding monomeric Pt(II) acetylides, the absorption bands of these Au(I)–Pt(II) polyynes show a weaker red shift than those of the homometallic Pt(II) polyynes (Fig. S2 and Table S1, ESI†). Therefore, these Au(I)–Pt(II) polyynes exhibit better transparency than homometallic Pt(II) polyynes, indicating the validity of introduction of Au(I) precursors with tetrahedral diphosphine ligands to improve transparency. The improvement of transparency can be attributed to the weak interaction between 5d orbitals of the Au(I) centers and π orbitals of the ethynyl aromatic ligands, as well as the conjugation-breaking ability of tetrahedral diphosphine ligands.

In the UV-Vis absorption spectra, all the Au(I)–Pt(II) polyynes exhibit intense absorption peaks with λ_{max} before 400 nm and a weak absorption tail after 400 nm (Fig. 1), indicating their excellent optical transparency in the visible light region (*ca.* 400–700 nm). Their intense absorption peaks can be mainly assigned to the metal disturbed π–π* transitions from the ethynyl aromatic ligands.[34] The profiles of P1 series and P2 series are similar in their absorption spectra. But the λ_{max} and $\lambda_{cut\text{-}off}$ in the absorption spectra of P2 series show a slight blue-shift compared with those of the corresponding P1 series, which is caused by the $-CH_2CH_2CH_2-$ group of **L-P2-Au** possessing a stronger conjugation-breaking ability. These results show that these new polyynes still maintain good transparency after polymerization. Besides, compared with the reported heterobimetallic Hg(II)–Pt(II) polyyne with fluorene-based ligands

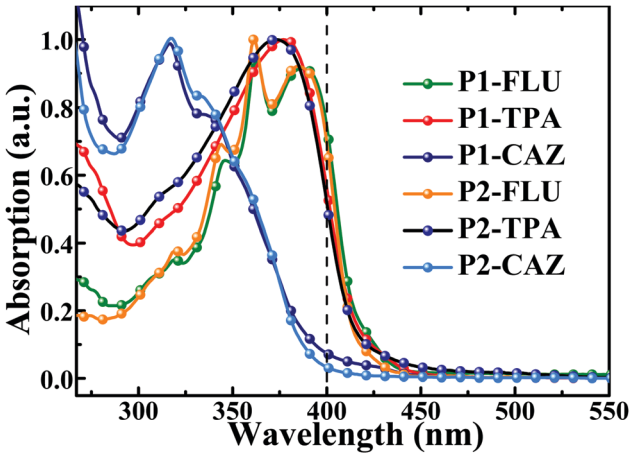

Fig. 1 UV-Vis absorption spectra for heterobimetallic Au(I)–Pt(II) polyynes in CH_2Cl_2 at 298 K.

($\lambda_{cut\text{-}off}$, 411 nm),[34] **P1-FLU**, **P1-TPA**, **P2-FLU** and **P2-TPA** (Table 1) can show comparable transparency and **P1-CAZ** and **P2-CAZ** (Table 1) can show better transparency in the visible-light region. Importantly, compared with the reported heterobimetallic Pd(II)–Pt(II) and Pd(II)–Hg(II) polyynes with fluorene-based ligands ($\lambda_{cut\text{-}off}$, 438 nm and 435 nm, respectively),[34] all the Au(I)–Pt(II) polyynes show much better transparency in the visible-light region.

Based on the fact that the transition properties of the transition metal polyynes can show similarity to their repeating units,[47] the molecular orbital (MO) patterns of the repeating units of these Au(I)–Pt(II) polyynes have been obtained by time-dependent density functional theory (TD-DFT) calculations to interpret their photophysical properties. Due to their large contribution to the transition of the S_1 states above 84% (Table 2), the transitions between the key molecular orbitals can represent the feature of the S_1 states of the repeating units for these Au(I)–Pt(II) polyynes. From the MO patterns of the Au(I)–Pt(II) polyynes (Fig. 2), their S_1 states should show obvious ligand–ligand charge transfer (LLCT) features from the π orbitals of diethynyl aromatic ligands to the π* orbitals of 1,4-bis(diphenylphosphino)benzene (**L-P1**)/1,3-bis(diphenylphosphino)propane (**L-P2**) ligands coordinated with the Au(I) centers.

Table 1 Photophysical data for heterobimetallic Au(I)–Pt(II) polyynes

Compound	Absorption[a] λ_{abs} (nm) 298 K	Emission[a] λ_{em} (nm) 298 K/77 K	Φ_F[b] (%)	Lifetime of excited states[c] S_1 state (ns)/T_1 state (μs)	$\lambda_{cut\text{-}off}$ (nm)
P1-FLU	270, 276, 305, 319, 345, 362, 387	417, 438, 450, 539/548, 587, 625, 642	1.03	0.71 ns (438 nm)/181.63 μs (548 nm)	416
P1-TPA	264, 276, 316^{sh}, 377	504/504, 545, 563	0.62	10.37 μs (504 nm)[d]/130.80 μs (504 nm)	414
P1-CAZ	253, 262, 276^{sh}, 317, 335	405, 425, 455, 495, 534/456, 492, 507, 527	0.27	0.99 ns (455 nm)/44.31 μs (456 nm)	389
P2-FLU	275, 305, 319, 344, 361, 384	412, 432, 449^{sh}, 542, 584/548, 586, 619	1.66	0.63 ns (412 nm)/137.84 μs (548 nm)	413
P2-TPA	268, 275, 314^{sh}, 373	504/503, 529, 603	1.69	6.46 μs (504 nm)[d]/165.23 μs (503 nm)	412
P2-CAZ	253, 261, 316, 334	402, 421, 438, 455, 503/457, 493, 507	0.30	0.72 ns (421 nm)/40.14 μs (457 nm)	386

[a] Measured in CH_2Cl_2 at a concentration of *ca.* 10^{-5} M. sh: shoulder. [b] Measured using quinine sulfate in 1.0 M H_2SO_4 as the standard. According to the UV-Vis absorption of the compounds, the excitation wavelengths were set at 334 nm and 365 nm while the Φ_F of the standard is 56% and 55%. [c] The numbers in parentheses are the emission wavelengths of the S_1 and T_1 states. The lifetime of the S_1 state was measured at 298 K in degassed CH_2Cl_2 with the excitation at 360 nm and that of the T_1 state was measured at 77 K in the same solvent with the same excitation wavelength. [d] The lifetime of **P1-TPA** and **P2-TPA** at 298 K should be a mixture of S_1 and T_1 states.

Table 2 TD-DFT results for heterobimetallic Au(I)–Pt(II) polyynes based on their optimized S_0 geometries

Compound	Contribution of d_π orbitals to the HOMO[a] (Pt/Au1/Au2)	Contribution of d_π orbitals to the LUMO[a] (Pt/Au1/Au2)	Largest coefficient in the CI expansion of the T_1 state[b]	Percentage contribution of the transition to the T_1 state[b]	Largest coefficient in the CI expansion of the S_1 state[b]	Percentage contribution of the transition to the S_1 state[b]	Oscillator strength (f) of the $S_0 \rightarrow S_1$ transition
P1-FLU	3.39/1.81/0%	0/2.08/2.84%	H → L (0.68291) 488 nm	93.27%	H → L (0.70015) 488 nm	98.04%	0.0156
P1-TPA	1.62/1.19/0%	0/1.11/1.22%	H → L (0.70346) 572 nm	98.97%	H → L (0.70410) 571 nm	99.15%	0.0016
P1-CAZ	7.50/1.16/0%	0/1.45/1.62%	H → L (0.69003) 498 nm	95.23%	H → L (0.69187) 498 nm	90.84%	0.0013
P2-FLU	3.23/1.99/0%	0/0.09/5.21%	H → L (0.70351) 442 nm	98.99%	H → L (0.70415) 442 nm	99.17%	0.0055
P2-TPA	2.05/1.15/0%	0/2.16/3.50%	H−1 → L (0.70366) 424 nm	99.03%	H → L (0.66865) 502 nm	89.42%	0.0066
P2-CAZ	5.02/1.03/0%	0/2.47/3.35%	H−1 → L+2 (0.66715) 382 nm	89.02%	H → L (0.65125) 454 nm	84.83%	0.0038

[a] The data were obtained by exporting DFT results using the software AOMix. [b] H–L represents the HOMO to LUMO transition. CI stands for configuration interaction.

The results of TD-DFT can give insight into the blue shift from P1 series to P2 series in the absorption process, which coincides well with the experimental results.

In CH_2Cl_2 solution at 298 K, the photoluminescent (PL) spectra of **P1-FLU** and **P2-FLU** exhibit two emission bands (Fig. 3a). The high-energy emission bands should be fluorescent signals from the radiative decay of the singlet states (S_1) associated with the metal disturbed organic ligand π–π* transitions. This result can be attributed to their short lifetime in the order of nanoseconds (ns). However, the long-wavelength emission bands should be induced by the decay of the triplet states (T_1) due to their longer lifetimes in the order of microseconds (μs) with large Stokes shift >100 nm. **P1-FLU** possesses stronger triplet emission compared with **P2-FLU**, which can be associated with its lower Φ_F (1.03% for **P1-FLU** and 1.66% for **P2-FLU**, Table 1). The PL spectra of **P1-CAZ** and **P2-CAZ** show two emission bands as well (Fig. 3c). It is obvious that **P1-CAZ** exhibits stronger triplet emission than **P2-CAZ**, which is also attributed to its lower Φ_F (0.27% for **P1-CAZ** and 0.30% for **P2-CAZ**). The PL spectra of **P1-TPA** and **P2-TPA** merely show one emission band at 298 K (Fig. 3b), but they should be the overlapping of singlet and triplet emission. This can be explained by the fact that **P1-TPA** and **P2-TPA** possess a long lifetime in the order of microseconds at 298 K (10.37 μs for **P1-TPA** and 6.46 μs for **P2-TPA**) and the emission bands of **P1-TPA** and **P2-TPA** at 77 K (Fig. S3b in the ESI†) completely overlap with the corresponding emission band at 298 K. Although the emission profiles of **P1-TPA** and **P2-TPA** are quite similar, the emission profile of **P1-TPA** becomes wider after 550 nm than that of **P2-TPA** (Fig. 3b). In addition, the Φ_F of **P1-TPA** (0.60%) is lower than that of **P2-TPA** (1.69%). So **P1-TPA** should possess stronger T_1 emission compared with **P2-TPA**. The improvement of triplet emission in P1 series might be related to the phenyl group of **L-P1-Au** that can extend the conjugation of the backbone in the Au(I)–Pt(II) polyynes. Furthermore, the feature of T_1 emission for these Au(I)–Pt(II) polyynes can also be obviously indicated by enhanced long-wavelength emission signals at 77 K.

In order to clearly interpret the PL behaviors of these Au(I)–Pt(II) polyynes, the natural transition orbital (NTO) results for their repeating units have been obtained based on the optimized T_1 geometries for the $S_0 \rightarrow T_1$ excitation.[40] The NTO patterns for the repeating unit of **P1-FLU** and **P2-FLU** (Fig. 4a and d) show that both hole (H) and particle (P) orbitals are mainly located on fluorene-based diethynyl ligands. Then, based on the large percentage of H → P transition for **P1-FLU** and **P2-FLU** (91.45% and 90.73%, respectively) (Table 3), they should indicate a ligand-centered ^{3}π–π* feature for the T_1 emission. However, the **L-P1** ligands of **P1-CAZ** and the **L-P2** ligands of **P2-CAZ** have noticeable contribution (62.62% and 61.67%, respectively) to the particles of the NTO patterns for their corresponding repeating units. So the T_1 emission of **P1-CAZ** and **P2-CAZ** should exhibit LLCT character. In addition, the T_1 emission of **P1-TPA** and **P2-TPA** also exhibits LLCT character due to the contribution of **L-P1** (63.3%) and **L-P2** (44.34%) to the particle of the NTO patterns for their corresponding repeating units. Due to the contribution (22.56%) of

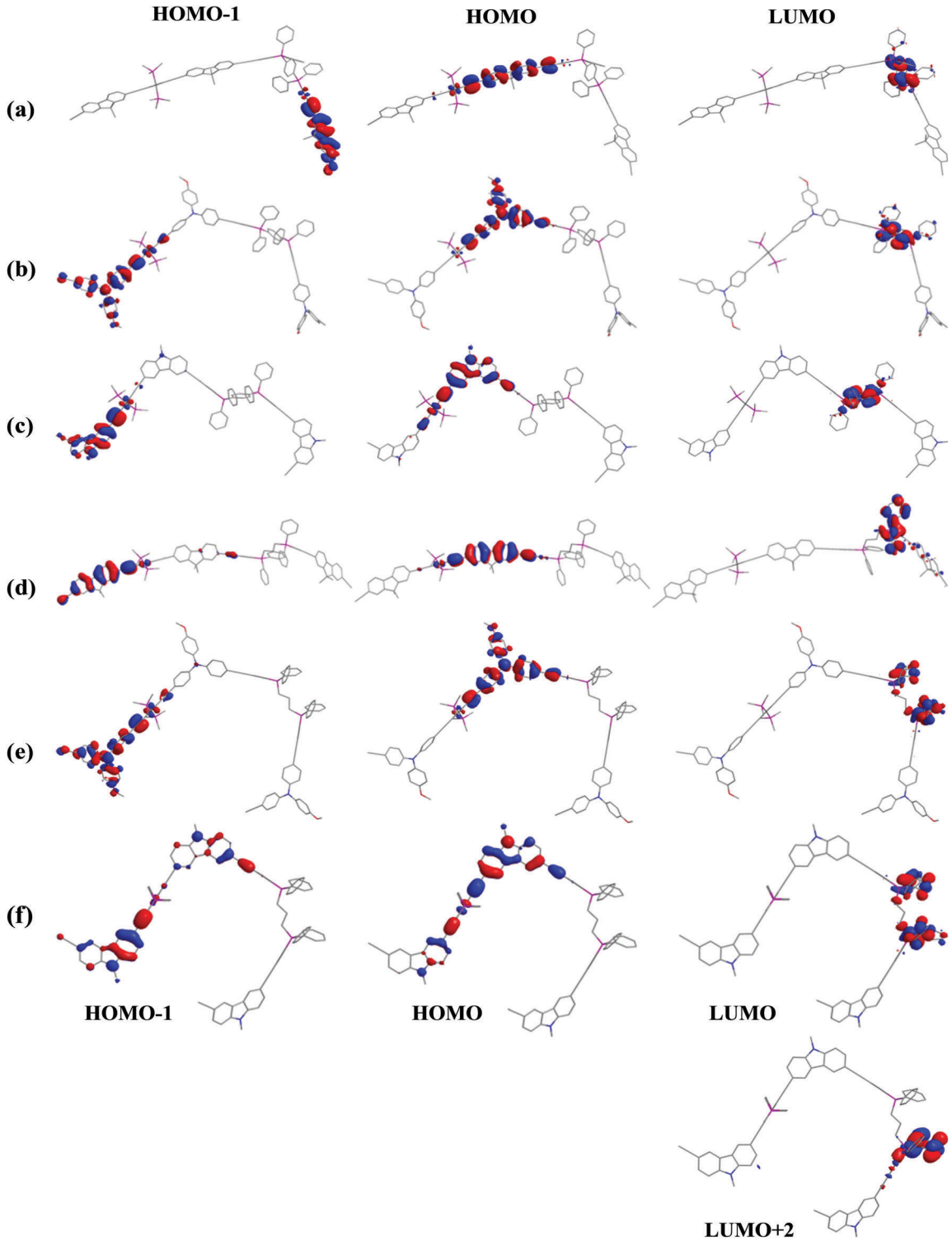

Fig. 2 Molecular orbital (MO) patterns for the repeating units of the heterobimetallic Au(I)–Pt(II) polyynes based on their optimized S_0 geometries. (a) Repeating unit for **P1-FLU**, (b) repeating unit for **P1-TPA**, (c) repeating unit for **P1-CAZ**, (d) repeating unit for **P2-FLU**, (e) repeating unit for **P2-TPA**, and (f) repeating unit for **P2-CAZ**.

the triphenylamine ligand, **P2-TPA** also shows a ligand-centered $^3\pi$–π^* feature for the T_1 emission. From the results of NTO in Table 3, the Au and Pt centers make negligible contribution to the transition process responsible for the T_1 emission of these Au(I)–Pt(II) polyynes. Moreover, the T_1 emission of these Au(I)–Pt(II) polyynes showing a ligand-centered $^3\pi$–π^* feature and LLCT characteristics can be indicated by the structured line-shape of their PL spectra at 77 K (Fig. S3, ESI†). The above

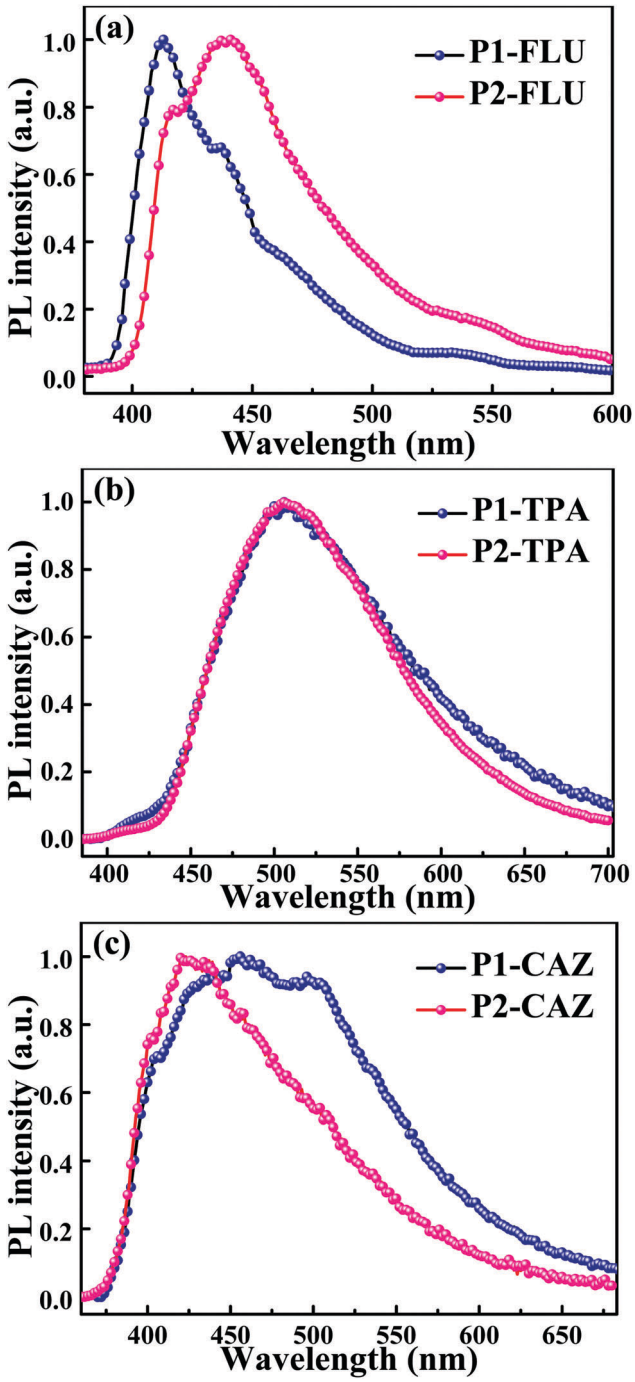

Fig. 3 Photoluminescent (PL) spectra for heterobimetallic Au(I)–Pt(II) polyynes in CH_2Cl_2 solution at 298 K. (a) **P1-FLU** and **P2-FLU** (b) **P1-TPA** and **P2-TPA** (c) **P1-CAZ** and **P2-CAZ**.

results demonstrate the good consistency between the experimental and theoretical results.

Optical power limiting behaviors

From their UV-Vis spectra, these Au(I)–Pt(II) polyynes show exceptional optical transparency at 532 nm, indicating their extremely low ground-state absorption at this wavelength. Their absorption behaviors fully meet the basic test requirements for characterizing their OPL properties against the 532 nm laser beam. Then the OPL behaviors of these Au(I)–Pt(II) polyynes have been characterized with a linear transmittance T_o of *ca.* 90% (Fig. 5) through the *Z*-scan with the open-aperture mode in CH_2Cl_2. Incident irradiance upon the Au(I)–Pt(II) polyynes varies from their *Z*-position to focal point ($Z = 0$). Obviously, the transmittance (T) of the sample in solution remains constant when the incident irradiance upon the sample is weak, showing linear optical properties (*i.e.* obeying Beer's law). However, when the sample gradually approaches the focus with an increase in incident irradiance, the transmittance (T) of the sample decreases to show an OPL effect (Fig. 5). The OPL behaviors of these Au(I)–Pt(II) polyynes can be interpreted by the reverse saturable absorption (RSA) mechanism of the T_1 states (Fig. S3, ESI†). Due to the strong SOC effect induced by the Au(I) and Pt(II) centers, the S_1 states formed through the weak absorption of laser irradiance can be rapidly transformed into the T_1 states through a fast inter-system crossing (ISC) process. After accumulating a certain population, these T_1 states absorb much more laser energy to reach the higher triplet state T_n to induce the OPL effect, especially for the nano-second laser pulse. The lifetime of the S_1 state is very short, so that the energy absorption from the $S_1 \rightarrow S_n$ transition can be neglected in the contribution to the nano-second OPL response. Therefore, the OPL ability mainly depends on the strong absorption from the $T_1 \rightarrow T_n$ transition, showing that these Au(I)–Pt(II) polyynes with a higher T_1 emission ability can show better OPL performances.

The OPL performances of these Au(I)–Pt(II) polyynes based on the reverse saturable absorption can be compared by using the figure of merit factor $\sigma_{ex}/\sigma_o = \ln T_{sat}/\ln T_o$, in which σ_o and σ_{ex} stand for the ground-state absorption cross-section and the effective excited-state absorption cross-section, respectively. T_o is the linear transmittance as aforementioned and T_{sat} is the transmittance at the saturation fluence. The σ_{ex}/σ_o values of **P1-FLU**, **P1-TPA** and **P1-CAZ** are 9.98, 8.39 and 4.01, respectively. The σ_{ex}/σ_o values of P2 series (7.92 for **P2-FLU**, 6.66 for **P2-TPA** and 3.72 for **P2-CAZ**) are lower than those of P1 series. Based on the RSA mechanism of T_1 states, the higher T_1 quantum yield associated with P1 series should enhance their OPL ability effectively. So the higher OPL behaviors of P1 series are correlated with their lower Φ_F at 298 K. Obviously, the performances of these Au(I)–Pt(II) polyynes are better than that of the state-of-the-art OPL material C_{60} (*ca.* 3.39), showing their great potential for application in the OPL field. In addition, compared with the reported heterobimetallic Hg(II)–Pt(II), Pd(II)–Pt(II) and Pd(II)–Hg(II) polyynes with fluorene-based ligands,[34] these Au(I)–Pt(II) analogs can successfully cope with the toxicity problem of the Hg(II) ions and the poor transparency-enhancing ability of the Pd(II) ions.

What is more, the σ_{ex}/σ_o values of two series of Au(I)–Pt(II) polyynes are higher than those of the corresponding homometallic Pt(II) polyynes (7.36 for **FLU-Pt**, 5.46 for **TPA-Pt** and 3.45 for **CAZ-Pt**) (Fig. S5, ESI†), indicating their better OPL behaviors. As mentioned before, the absorption bands of two series of Au(I)–Pt(II) polyynes show a blue shift compared with the corresponding homometallic Pt(II) polyynes, showing enhanced

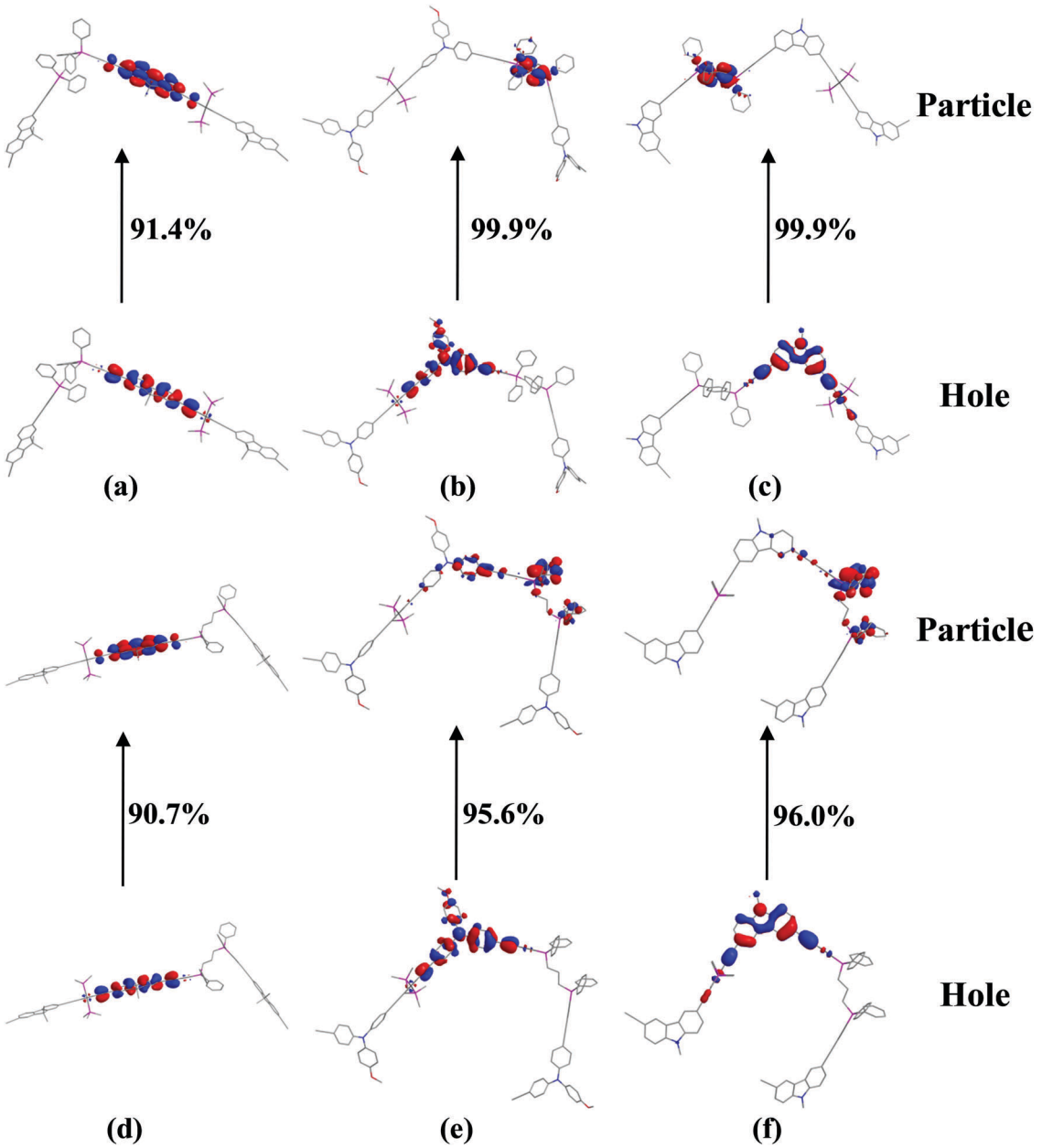

Fig. 4 Natural transition orbital (NTO) patterns for $S_0 \rightarrow T_1$ excitation of the repeating units from the heterobimetallic Au(I)–Pt(II) polyynes based on their optimized T_1 geometries. (a) Repeating unit for **P1-FLU**, (b) repeating unit for **P1-TPA**, (c) repeating unit for **P1-CAZ**, (d) repeating unit for **P2-FLU**, (e) repeating unit for **P2-TPA**, and (f) repeating unit for **P2-CAZ**.

transparency. Therefore, these results fully illustrate that introducing Au(I) precursors with tetrahedral diphosphine ligands into the backbone of homometallic Pt(II) polyynes successfully achieve a good trade-off between transparency and optical power limiting performance.

Because OPL materials in solution are inconvenient to make practical devices, it is highly valuable to use them in the solid state. **P1-FLU** and **P2-FLU** have been doped into polystyrene (PS) with a *ca.* 1.0 wt% doping level to make two prototype devices to characterize its OPL ability for the 532 nm laser. The prepared doped PS thin plates with a thickness of 0.2 mm show very high transparency, possessing a linear transmittance of *ca.* 80% (81% for **P1-FLU** and 82% for **P2-FLU**) (inset Fig. 6), respectively. As the input fluence increases, the normalized transmittance of the **P1-FLU** doped PS plate continuously drops to 0.48, reaching an OPL threshold of *ca.* 0.18 J cm^{-2}, while that of the **P2-FLU** doped PS plate is *ca.* 0.2 J cm^{-2}. Obviously, as a prototype OPL device, the **P1-FLU** doped PS plate shows enhanced OPL ability compared to the **P2-FLU** doped PS plate, which is similar to their OPL performance in solution. In addition, the PL spectra of **P1-FLU** and **P2-FLU** in the PS matrix (Fig. S6, ESI†) show stronger T_1 emission than those of their corresponding solutions, indicating their advantage in the fabrication of OPL devices.

Table 3 NTO results for repeating units from the heterobimetallic Au(I)–Pt(II) polyynes based on their optimized T_1 geometries

Compound	NTO[a]	Contribution percentages of metal d_π orbitals and π orbitals of ligands to NTOs[b] (%)				
		Pt	Au1	Au2	L1	L2
P1-FLU	H	1.28	1.87	0.00	95.54	0.00
	P	0.54	5.27	0.06	87.81	1.80
P1-TPA	H	1.25	1.70	0.00	95.66	0.07
	P	0.00	1.51	1.11	0.56	63.32
P1-CAZ	H	5.16	2.25	0.00	87.30	0.08
	P	0.00	2.06	1.44	0.70	62.62
P2-FLU	H	1.25	1.87	0.00	95.60	0.19
	P	0.64	5.02	0.01	91.39	1.77
P2-TPA	H	1.24	1.88	0.00	95.36	0.25
	P	0.30	8.55	1.31	25.56	44.34
P2-CAZ	H	2.46	2.70	0.00	87.53	0.37
	P	0.01	7.03	1.44	7.77	61.67

[a] H and P represent the NTO hole and particle orbital, respectively. [b] Pt represents the Pt(II) centers, and Au1 and Au2 represent the two Au(I) centers, while L1 indicates the aromatic diacetylene ligands and L2 represents the organic phosphine ligands (**L-P1** and **L-P2**).

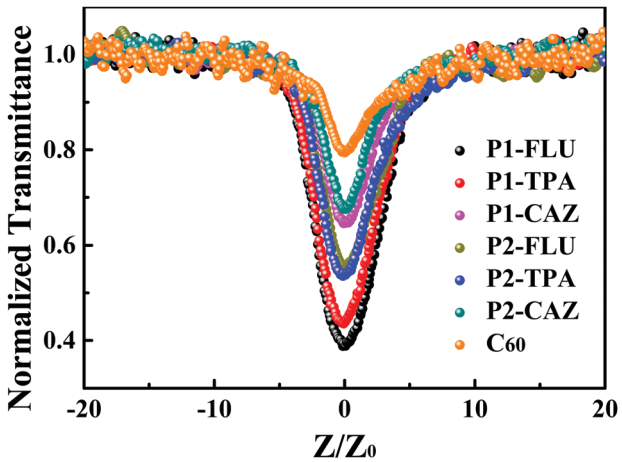

Fig. 5 Open-aperture Z-scan results for heterobimetallic Au(I)–Pt(II) polyynes (T_o *ca.* 90%) together with that for C_{60} (T_o *ca.* 89%).

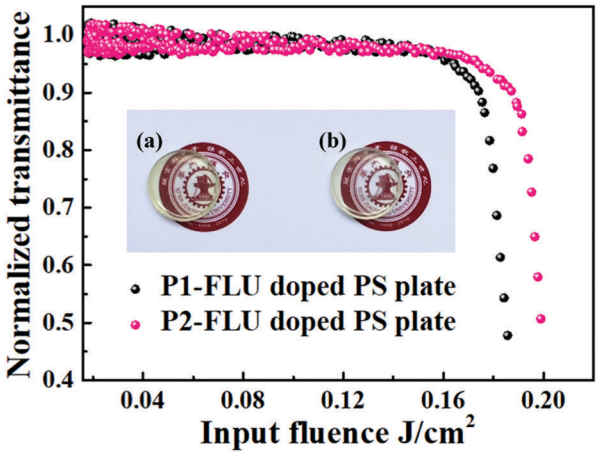

Fig. 6 Normalized transmittance of the **P1-FLU** and **P2-FLU** (T_o *ca.* 80%) doped PS plate. (a) **P1-FLU** doped PS plate and (b) **P2-FLU** doped PS plate.

Conclusions

Two series of heterobimetallic Au(I)–Pt(II) polyynes have been successfully prepared. On the premise of transparency approximation of two series of Au(I)–Pt(II) polyynes, P1 series exhibit stronger T_1 emission and superior OPL performances than P2 series. This result indicates that the 1,4-bis(diphenylphosphino)-benzene ligand is more favorable for optimizing the optical transparency and OPL ability of OPL materials than the 1,3-bis-(diphenylphosphino)propane ligand. Importantly, the absorption bands of these Au(I)–Pt(II) polyynes are blue-shifted by introducing Au(I) precursors with tetrahedral phosphine ligands into the homometallic Pt(II) polyynes backbone, indicating better transparency in the visible-light region. Moreover, the OPL performances of these polyynes are not only superior to the corresponding homometallic Pt(II) polyynes, but also outperform the state-of-the-art OPL material C_{60}. When compared with the reported heterobimetallic polyynes with fluorene-based ligands, the heterobimetallic Au(I)–Pt(II) polyynes with fluorene-based ligands show a lower toxicity and even achieve consistency between excellent, good transparency and high OPL performances. The concerned results provide valuable information for the comprehensive optimization of OPL materials.

Conflicts of interest

There are no conflicts to declare.

Acknowledgements

This research was financially supported by the National Natural Science Foundation of China (no. 21572176 and 21602170), the Fundamental Research Funds for the Central Universities (cxtd2015003 and xjj2016061), the Key Creative Scientific Research Team in Yulin City, Shaanxi Province, the China Postdoctoral Science Foundation (2015M580831) and the Program for New Century Excellent Talents in University, the Ministry of Education of China (NECT-09-0651). The financial support from the State Key Laboratory for Mechanical Behavior of Materials is also acknowledged. The characterizations of materials are supported by the Instrument Analysis Center of Xi'an Jiaotong University.

Notes and references

1 J. Hecht, *Opt. Eng.*, 2010, **49**, 99.
2 C. W. Spangler, *J. Mater. Chem.*, 1999, **9**, 2013.
3 L. W. Tutt and T. F. Boggess, *Prog. Quantum Electron.*, 1993, **17**, 299.
4 X. Liu, D. Wang, H. Gao, Z. Yang, Y. Xing, H. Cao, W. He, H. Wang, J. Gu and H. Hu, *Phys. Chem. Chem. Phys.*, 2016, **18**, 7341.
5 A. Y. Tolbin, A. V. Dzuban, E. V. Shulishov, L. G. Tomilova and N. S. Zefirov, *New J. Chem.*, 2016, **40**, 8262.
6 P. Zhao, Z. Wang, J. Chen, Y. Zhou and F. Zhang, *Opt. Mater.*, 2017, **66**, 98.

7 N. V. Krishna, P. T. Anusha, S. V. Rao and L. Giribabu, *J. Porphyrins phthalocyanines*, 2016, **20**, 1173.
8 X. Liu, D. Wang, H. Gao, Z. Yang, Y. Xing, H. Cao, W. He, H. Wang, J. Gu and H. Hu, *Dyes Pigm.*, 2016, **134**, 155.
9 D. Dini, M. J. F. Calvete and M. Hanack, *Chem. Rev.*, 2016, **116**, 13043.
10 K. M. Hijas, S. M. Kumar, K. Byrappa, T. Geethakrishnan, S. Jeyaram and R. Nagalakshmi, *J. Mol. Struct.*, 2018, **1155**, 249.
11 Z. Xiao, Y. Shi, R. Sun, J. Ge, Z. Li, Y. Fang, X. Wu, J. Yang, M. Zhao and Y. Song, *J. Mater. Chem. C*, 2016, **4**, 4647.
12 C. R. Ma, J. Xiao and G. W. Yang, *J. Mater. Chem. C*, 2016, **4**, 4692.
13 Y. Du, N. Dong, M. Zhang, K. Zhu, R. Na, S. Zhang, N. Sun, G. Wang and J. Wang, *Phys. Chem. Chem. Phys.*, 2017, **19**, 2252.
14 R. Liu, J. Hu, S. Zhu, J. Lu and H. Zhu, *ACS Appl. Mater. Interfaces*, 2017, **9**, 33029.
15 Y. Xiong, J. Si, L. Yan, H. Song, W. Yi and X. Hou, *Laser Phys. Lett.*, 2014, **11**, 115904.
16 G. Zhou and W.-Y. Wong, *Chem. Soc. Rev.*, 2011, **40**, 2541.
17 W. Wang, L. J. Chen, X. Q. Wang, B. Sun, X. Li, Y. Zhang, J. Shi, Y. Yu, L. Zhang, M. Liu and H. B. Yang, *Proc. Natl. Acad. Soc. U. S. A.*, 2015, **112**, 5597.
18 B. Jiang, J. Zhang, J. Q. Ma, W. Zheng, L. J. Chen, B. Sun, C. Li, B. W. Hu, H. Tan, X. Li and H. B. Yang, *J. Am. Chem. Soc.*, 2016, **138**, 738.
19 L. Xu and H. B. Yang, *Chem. Rec.*, 2016, **16**, 1274.
20 W. Wang and H. B. Yang, *Chem. Commun.*, 2014, **50**, 5171.
21 H. Zhang, X. Yan, J. Zhao, X. Yang, Z. Huang, G. Zhou and Y. Wu, *RSC Adv.*, 2015, **5**, 88758.
22 Z. Huang, B. Liu, Y. He, X. G. Yan, X. Yang, X. Xu, G. Zhou, Y. Ren and Z. Wu, *J. Organomet. Chem.*, 2015, **794**, 1.
23 W.-Y. Wong and C.-L. Ho, *Acc. Chem. Res.*, 2010, **43**, 1246.
24 B. Jiang, L. J. Chen, G. Q. Yin, Y. X. Wang, W. Zheng, L. Xu and H. B. Yang, *Chem. Commun.*, 2017, **53**, 172.
25 I. R. Whittall, M. G. Humphrey, S. Houbrechts, J. Maes, A. Persoons, S. Schmid and D. C. R. Hockless, *J. Organomet. Chem.*, 1997, **544**, 277.
26 N. J. Long, *Angew. Chem., Int. Ed. Engl.*, 1995, **34**, 21.
27 S. Goswami, G. Wicks, A. Rebane and K. S. Schanze, *Dalton Trans.*, 2014, **43**, 17721.
28 Y. Du, N. Dong, M. Zhang, B. Jiang, N. Sun, Y. Luo, S. Zhang, G. Wang and J. Wang, *J. Mater. Chem. C*, 2018, **6**, 7317.
29 T. Kindahl, P. G. Ellingsen, C. Lopes, C. Brannlund, M. Lindgren and B. Eliasson, *J. Phys. Chem. A*, 2012, **116**, 11519.
30 T. Kindahl, J. Öhgren, C. Lopes and B. Eliasson, *Tetrahedron Lett.*, 2013, **54**, 2403.
31 B. Liu, Z. Tian, F. Dang, J. Zhao, X. Yan, X. Xu, X. Yang, G. Zhou and Y. Wu, *J. Organomet. Chem.*, 2016, **804**, 80.
32 K. B. Manjunatha, V. M. Shelar, R. Dileep, G. Umesh, M. N. Satyanarayan and B. R. Bhat, *Synth. React. Inorg. Met.-Org. Chem.*, 2014, **44**, 282.
33 W.-Y. Wong, L. Liu and J.-X. Shi, *Angew. Chem., Int. Ed.*, 2003, **42**, 4064.
34 G. Zhou, W.-Y. Wong, C. Ye and Z. Lin, *Adv. Funct. Mater.*, 2007, **17**, 963.
35 P. I. P. Elliott, *Annu. Rep. Prog. Chem., Sect. A: Inorg. Chem.*, 2012, **108**, 389.
36 W.-Y. Wong, *J. Inorg. Organomet. Polym. Mater.*, 2005, **15**, 197.
37 W.-Y. Wong, S.-Y. Poon, A. W. Lee, J.-X. Shi and K.-W. Cheah, *Chem. Commun.*, 2004, 2420.
38 D. W. Boening, *Chemosphere*, 2000, **40**, 1335.
39 L. Liu, W.-Y. Wong, S.-Y. Poon, J.-X. Shi, K.-W. Cheah and Z. Lin, *Chem. Mater.*, 2006, **18**, 1369.
40 Z. Tian, X. Yang, B. Liu, J. Zhao, D. Zhong, Y. Wu, G. Zhou and W.-Y. Wong, *J. Mater. Chem. C*, 2018, **6**, 6023.
41 W. R. Dawson and M. W. Windsor, *J. Phys. Chem.*, 1968, **72**, 3251.
42 W. R. Wadt and P. J. Hay, *J. Chem. Phys.*, 1985, **82**, 284.
43 P. J. Hay and W. R. Wadt, *J. Chem. Phys.*, 1985, **82**, 299.
44 M. J. Frisch, G. W. Trucks, H. B. Schlegel, G. E. Scuseria, M. A. Robb, J. R. Cheeseman, J. A. Montgomery, T. Vreven Jr, K. N. Kudin, J. C. Burant, J. M. Millam, S. S. Iyengar, J. Tomasi, V. Barone, B. Mennucci, M. Cossi, G. Scalmani, N. Rega, G. A. Petersson, H. Nakatsuji, M. Hada, M. Ehara, K. Toyota, R. Fukuda, J. Hasegawa, M. Ishida, T. Nakajima, Y. Honda, O. Kitao, H. Nakai, M. Klene, X. Li, J. E. Knox, H. P. Hratchian, J. B. Cross, V. Bakken, C. Adamo, J. Jaramillo, R. Gomperts, R. E. Stratmann, O. Yazyev, A. J. Austin, R. Cammi, C. Pomelli, J. W. Ochterski, P. Y. Ayala, K. Morokuma, G. A. Voth, P. Salvador, J. J. Dannenberg, V. G. Zakrzewski, S. Dapprich, A. D. Daniels, M. C. Strain, O. Farkas, D. K. Malick, A. D. Rabuck, K. Raghavachari, J. B. Foresman, J. V. Ortiz, Q. Cui, A. G. Baboul, S. Clifford, J. Cioslowski, B. B. Stefanov, G. Liu, A. Liashenko, P. Piskorz, I. Komaromi, R. L. Martin, D. J. Fox, T. Keith, M. A. Al-Laham, C. Y. Peng, A. Nanayakkara, M. Challacombe, P. M. W. Gill, B. Johnson, W. Chen, M. W. Wong, C. Gonzalez and J. A. Pople, *Gaussian 09, revision A.2*, Gaussian, Inc., Wallingford, CT, 2009.
45 C. K. Mirabelli, D. T. Hill, L. F. Faucette, F. L. McCabe, G. R. Girard, D. B. Bryan, B. M. Sutton, J. O. Bartus, S. T. Crooke and R. K. Johnsonl, *J. Med. Chem.*, 1987, **30**, 2181.
46 M.-C. Brandys, M. C. Jennings and R. J. Puddephatt, *J. Chem. Soc., Dalton Trans.*, 2000, **24**, 4601.
47 G. Zhou, Y. He, B. Yao, J. Dang, W.-Y. Wong, Z. Xie, X. Zhao and L. Wang, *Chem. – Asian J.*, 2010, **5**, 2405.

